9

Life Prediction of Gas Turbine Materials

Xijia Wu
Institute for Aerospace Research, National Research Council
Canada

1. Introduction

The advance of gas turbine engines and the increase in fuel efficiency over the past 50 years relies on the development of high temperature materials with the performance for the intended services. The cutaway view of an aero engine is shown in Fig. 1. During the service of an aero engine, a multitude of material damage such as foreign object damage, erosion, high cycle fatigue, low cycle fatigue, fretting, hot corrosion/oxidation, creep, and thermomechanical fatigue will be induced to the components ranging from fan/compressor sections up front to high pressure (HP) and low pressure (LP) turbine sections at the rear. The endurance of the gas turbine engine to high temperature is particularly marked by the creep resistance of HP turbine blade alloy. Figure 2 shows the trend of firing temperature and turbine blade alloy capability (Schilke, 2004). Nowadays, the state-of-the-art turbine blade alloys are single crystal Ni-base superalloys, which are composed of intermetallic γ' (Ni_3Al) precipitates in a solution-strengthened γ matrix, solidified in the [100] crystallographic direction. Turbine disc alloys are also mostly polycrystalline Ni-base superalloys, produced by wrought or powder metallurgy processes. Compressor materials can range from steels to titanium alloys, depending on the cost or weight-saving concerns in land and aero applications. Coatings are often applied to offer additional protection from thermal, erosive and corrosive attacks. In general, the advances in gas turbine materials are often made through thermomechanical treatments and/or compositional changes to suppress the failure modes found in previous services, since these materials inevitably incur service-induced degradation, given the hostile (hot and corrosive) operating environment. Therefore, the potential failure mechanisms and lifetimes of gas turbine materials are of great concern to the designers, and the hot-section components are mostly considered to be critical components from either safety or maintenance points of view.

Because of its importance, the methodology of life prediction has been under development for many decades (see reviews by Viswanathan, 1989; Wu et al., 2008). The early approaches were mainly empirically established through numerous material and component tests. However, as the firing temperatures are increased and the operating cycles become more complicated, the traditional approaches are too costly and time-consuming to keep up with the fast pace of product turn-around for commercial competition. The challenges in life prediction for gas turbine components indeed arise due to their severe operating conditions: high mechanical loads and temperatures in a high-speed corrosive/erosive gaseous environment. The combination of thermomechanical loads and a hostile environment may induce a multitude of material damages including low-cycle fatigue, creep, fretting and oxidation. Gas turbine designers need analytical methods to extrapolate the limited material

property data, often generated from laboratory testing, to estimate the component life for the design operating condition. Furthermore, the requirement of accurate and robust life prediction methods also comes along with the recent trend of prognosis and health management, where assessment of component health conditions with respect to the service history and prediction of the remaining useful life are needed in order to support automated mission and maintenance/logistics planning.

To establish a physics-based life prediction methodology, in this chapter, the fundamentals of high temperature deformation are first reviewed, and the respective constitutive models

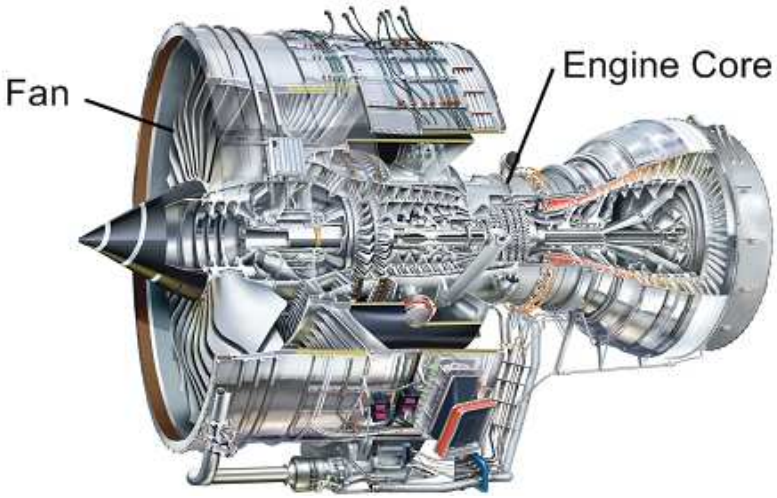

Fig. 1. Cutaway view of the Rolls-Royce Trent 900 turbofan engine used on the Airbus A380 family of aircraft (Trent 900 Optimised for the Airbus A380 Family, Rolls-Royce Plc, Derby UK, 2009).

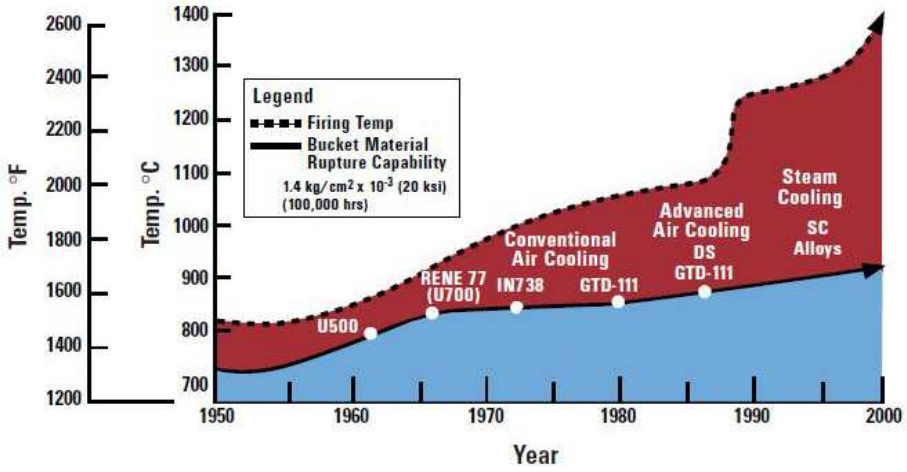

Fig. 2. Increase of firing temperature with respect to turbine blade alloys development (Schilke, 2004).

are introduced. Then, the evolution of material life by a combination of damage mechanisms is discussed with respect to general thermomechanical loading. Furthermore, crack growth problems and the damage tolerance approach are also discussed with the application of fracture mechanics principles.

2. Fundamentals of high temperature deformation

In general, for a polycrystalline material, deformation regimes can be summarized by a deformation map, following Frost and Ashby (Frost & Ashby, 1982), as shown schematically in Fig. 3. Elastic (E) and rate-independent plasticity (P) usually happens at low temperatures (i.e. $T < 0.3\ T_m$, where T_m is the melting temperature). In the plasticity regime, the deformation mechanism is understood to be dislocation glide, shearing or looping around the obstacles along the path; and the material failure mechanism mainly occurs by alternating slip and slip reversal, leading to fatigue, except for ultimate tensile fracture and brittle fracture. As temperature increases, dislocations are freed by vacancy diffusion to get around the obstacles so that time-dependent deformation manifests. Time dependent deformation at elevated temperatures is basically assisted by two diffusion processes—grain boundary diffusion and lattice diffusion. The former process assists dislocation climb and glide along grain boundaries, resulting in grain boundary sliding (GBS), whereas the latter process assists dislocation climb and glide within the grain interior, resulting in intragranular deformation (ID) such as the power-law and power-law-breakdown.

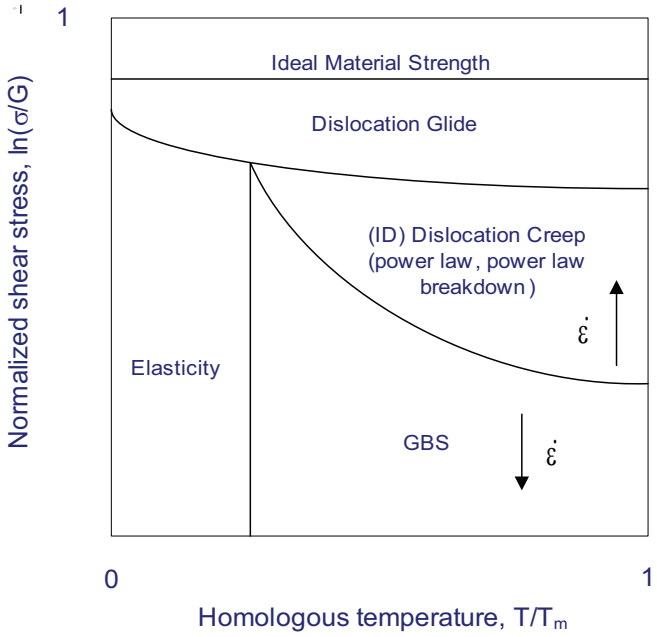

Fig. 3. A schematic deformation mechanism map.

In an attempt to describe inelastic deformation over the entire stress-temperature field, several unified constitutive laws have been proposed, e.g. Walker (1981), Chaboche & Gailetaud (1986), and most recently, Dyson & McLean (2000). These constitutive models

employ a set of evolution rules for kinematic and isotropic hardening to describe the total viscoplastic response of the material, but do not necessarily differentiate whether the contribution comes from intrgranular deformation mechanism or GBS, and hence have limitations in correlating with the transgranular, intergranular and/or mixed failure modes that commonly occur in gas turbine components. Therefore, a physics-based theoretical framework encompassing the above deformation and damage mechanisms is needed.
To that end, we proceed with the basic concept of strain decomposition that the total inelastic strain in a polycrystalline material can be considered to consist of intragranular strain ε_g and grain boundary sliding ε_{gbs}, as:

$$\varepsilon_{in} = \varepsilon_g + \varepsilon_{gbs} \tag{1}$$

The physics-based strain decomposition rule, Eq. (1), with the associated deformation mechanisms is the foundation for the development of an integrated creep-fatigue (ICF) modelling framework as outlined in the following sections (Wu et al. 2009).

2.1 Intragranular deformation

Intragranular deformation can be viewed as dislocation motion, which may occur by glide at low temperatures and climb plus glide at high temperatures, overcoming the energy barriers of the lattice. By the theory of deformation kinetics (Krausz & Eyring, 1975), the rate of the net dislocation movement can be formulated as a hyperbolic sine function of the applied stress (Wu & Krausz, 1994). In keeping consistency with the Prandtl-Reuss-Drucker theory of plasticity, the flow rule of intragranular strain, in tensor form, can be expressed as

$$\dot{\boldsymbol{\varepsilon}}_g = \dot{p}_g \boldsymbol{n}_g \tag{2}$$

where $\dot{p}_g$ is the plastic multiplier as defined by

$$\dot{p}_g = 2A(1 + Mp_g)\sinh(\psi) = \sqrt{\tfrac{2}{3}\dot{\boldsymbol{\varepsilon}}_g : \dot{\boldsymbol{\varepsilon}}_g} \tag{3}$$

where A is an Arrhenius-type rate constant, M is a dislocation multiplication factor, and $\boldsymbol{n}_g$ is the flow direction as defined by

$$\boldsymbol{n}_g = \frac{3}{2}\frac{(\boldsymbol{s} - \boldsymbol{\chi}_g)}{\sigma_g^{eq}} \tag{4}$$

where $\mathbf{s}$ is the deviatoric stress tensor and χ_g is the back stress tensor.
Note that the stress and temperature dependence of the plastic multiplier is described by a hyperbolic sine function, Eq. (3), with the evolution of activation energy ψ given by:

$$\dot{\psi} = \frac{V}{kT}\dot{\sigma}_g^{eq} \tag{5}$$

where V is the activation volume, k is the Boltzmann constant, and T is the absolute temperature in Kelvin. Eq. (3) covers both the power-law and the power-law-breakdown regimes in Fig. 3.
As intragranular deformation proceeds, a back stress may arise from competition between work hardening (dislocation pile-up and network formation) and recovery (dislocation climb) as:

$$\dot{\chi}_g = \frac{2}{3} H_g \dot{\varepsilon}_g - \kappa \chi_g \tag{6}$$

where H_g is the work-hardening coefficient and κ is the climb rate (see detailed formulation later). Note that more complicated expressions that consider both hardening and dynamic/static recovery terms may need to be used to formulate the back stress with large deformation and microstructural changes, but to keep the simplicity for small-scale deformation (<1%), Eq. (6) is suffice, as demonstrated in the later examples.
The effective equivalent stress for intragranular deformation is given by

$$\sigma_g^{eq} = \sqrt{\frac{3}{2}\left(\boldsymbol{s} - \boldsymbol{\chi}_g\right) : \left(\boldsymbol{s} - \boldsymbol{\chi}_g\right)} \tag{7}$$

where the column (:) signifies tensor contraction.

2.2 Grain boundary sliding

Based on the grain boundary dislocation glide-climb mechanism in the presence of grain boundary precipitates (Wu & Koul, 1995; 1997), the governing flow equation for GBS can be expressed as

$$\dot{\boldsymbol{\varepsilon}}_{gbs} = \dot{p}_{gbs} \boldsymbol{n}_{gbs} \tag{8}$$

with a GBS multiplier as defined by

$$\dot{p}_{\text{gbs}} = \varphi \frac{D\mu b}{kT} \left(\frac{b}{d}\right)^q \left(\frac{l+r}{b}\right)^{q-1} \frac{\left(\sigma_{gbs}^{eq}\right)\left(\sigma^{eq} - \sigma_{ic}\right)}{\mu^2} \tag{9}$$

where D is the diffusion constant, μ is the shear modulus, and b is the Burgers vector, d is the grain size, r is the grain boundary precipitate size, l is the grain boundary precipitate spacing, and q is the index of grain boundary precipitate distribution morphology (q = 1 for clean boundary, q =2 for discrete distribution, and q = 3 for a network distribution). The GBS flow direction is defined by

$$\boldsymbol{n}_{gbs} = \frac{3}{2} \frac{\left(\boldsymbol{s} - \boldsymbol{\chi}_{gbs}\right)}{\sigma_{gbs}^{eq}} \tag{10}$$

The two equivalent stresses in Eq. (9) are given by

$$\sigma_{gbs}^{eq} = \sqrt{\frac{3}{2}\left(\boldsymbol{s} - \boldsymbol{\chi}_{gbs}\right) : \left(\boldsymbol{s} - \boldsymbol{\chi}_{gbs}\right)} \tag{11}$$

and

$$\sigma^{eq} = \sqrt{\frac{3}{2}\boldsymbol{s} : \boldsymbol{s}} \tag{12}$$

The evolution of the grain boundary back stress in the presence of grain boundary precipitates is given by (Wu & Koul, 1995)

$$\dot{\boldsymbol{\chi}}_{gbs} = \frac{2}{3} H_{gbs} \dot{\boldsymbol{\varepsilon}}_{gbs} - \kappa \boldsymbol{\chi}_{gbs} \tag{13}$$

where H_{gbs} is the grain boundary work hardening coefficient, and κ is the dislocation climb rate as given by

$$\kappa = \frac{D\mu b}{kT} \frac{(\sigma^{eq} - \sigma_{ic})}{\mu} \tag{14}$$

The equivalent stress for GBS, σ_{gbs}^{eq}, controls the grain boundary dislocation glide with a back stress χ_{gbs}. The other equivalent stress, σ^{eq}, controls grain boundary dislocation climb, once it surpass a threshold stress, σ_{ic}, that arises from the constraint of grain boundary precipitates. As shown in Eq. (9), the GBS multiplier is controlled by the grain boundary diffusion constant D and grain boundary microstructural features such as the grain size, the grain boundary precipitate size and spacing, and their morphology. The back stress formulation, Eq. (13), states the competition between dislocation glide, which causes grain boundary dislocation pile-up, and recovery by dislocation climb. Henceforth, Eq. (9) depicts the grain boundary plastic flow as a result of dislocation climb plus glide overcoming the microstructural obstacles present at the grain boundaries. Last but not least, GBS is also affected by the grain boundary waveform, as given by the factor ϕ (Wu & Koul, 1997):

$$\phi = \begin{cases} \dfrac{2}{1 + \left(\dfrac{2h}{\lambda}\right)^2} - 1 & \textit{for triangular boundaries} \\ \dfrac{2}{\sqrt{1 + \left(\dfrac{\pi h}{\lambda}\right)^2}} - 1 & \textit{for sinusoidal boundaries} \end{cases} \tag{15}$$

where λ is wavelength and h is the amplitude.
By solving all the components of inelasticity, the evolution of the stress tensor is governed by

$$\dot{\boldsymbol{\sigma}} = \boldsymbol{C} : (\dot{\boldsymbol{\varepsilon}} - \dot{\boldsymbol{\varepsilon}}_{in}) \tag{16}$$

3. Deformation processes and constitutive models

3.1 Cyclic deformation and fatigue

It is commonly known that a metal subjected to repetitive or flunctuating stress will fail at a stress much lower than its ultimate strength. Failures occuring under cyclic loading are generally termed *fatigue*. The underlying mechanisms of fatigue is dislocation glide, leading to formation of persistent slip bands (PBS) and a dislocation network in the material. Persistent slip bands, when intersecting at the interface of material discontinuities (surface, grain boundaries or inclusions, etc.) result in intrusions/extrusions or dislocation pile-ups, inevitably leading to crack nucleation.
To describe the process of cyclic deformation, we start with tensile deformation as follows.
For uniaxial strain-controlled loading, the deformation is constrained as:

$$\dot{\varepsilon} = \frac{\dot{\sigma}}{E} + \dot{\varepsilon}_p = \text{constant} \tag{17}$$

Substituting Eq. (3-7) into Eq. (17) (neglecting dislocation climb, i.e., $\kappa\chi_g << H\dot{\varepsilon}$; and multiplication, i.e., M = 0), we have the first-order differential equation of Ψ, as (Wu et al., 2001)

$$\dot{\Psi} = \frac{EV}{kT}\left[\dot{\varepsilon} - 2A\left(1+\frac{H}{E}\right)\sinh\Psi\right] \tag{18}$$

which can be solved as

$$\left(\frac{e^{-\Psi}-a}{\chi e^{-\Psi}+b}\right) = \left(\frac{1-a}{\chi+b}\right)\exp\left\{-\frac{VE\dot{\varepsilon}(t-t_0)\sqrt{1+\chi^2}}{kT}\right\} \tag{19}$$

where

$$\chi = \frac{2A}{\dot{\varepsilon}}\left(1+\frac{H}{E}\right),\quad a = \frac{\sqrt{1+\chi^2}-1}{\chi},\quad b = \sqrt{1+\chi^2}+1 \tag{20}$$

The initial time of plastic deformation is defined by

$$\Psi_0 = \frac{(\sigma - H\varepsilon_p^0 - \sigma_0)}{kT} = 0 \tag{21}$$

where ε^0_p is the plastic strain accumulated from the prior deformation history, and σ_0, as an integration constant, represents the initial lattice resistance to dislocation glide. At the first loading, $\varepsilon^0_p = 0$. Since the deformation is purely elastic before the condition, Eq. (21), is met: $\sigma = E\dot{\varepsilon}t$, then $t_0 = \sigma_0/(E\dot{\varepsilon})$. Once the stress exceeds the initial lattice resistance in the material, i.e., $\sigma > \sigma_0$, plasticity commences. In this sense, σ_0 corresponds to the critial resolved shear stress by a Taylor factor.

From Eq. (20), we can obtain the stress-strain response as follows:

$$\sigma - H\varepsilon_p - \sigma_0 = -\frac{kT}{V}\ln\left(\frac{a+\omega(\varepsilon)b}{1-\omega(\varepsilon)\chi}\right) \tag{22}$$

where, ω(ε) is a response function as defined by

$$\omega(\varepsilon) = \left(\frac{1-a}{\chi+b}\right)\exp\left\{-\frac{V(E\varepsilon-\sigma_0)\sqrt{1+\chi^2}}{kT}\right\} \tag{23}$$

Eq. (22) basically describes the accumulation of plastic strain via the linear strain-hardening rule with dislocation glide as the dominant process and limited dislocation climb activities. It is applicable to high strain rate loading conditions, which are often encountered during engine start-up and shutdown or vibration conditions caused by mechanical and/or aerodynamic forces.

Based on the deformation kinetics, Eq. (22) describes the time and temperature dependence of high temperature deformation. As an example, the tensile behaviors of IN738LC at 750 °C, 850 °C and 950 °C are described using Eq. (22) and shown in Fig. 4, in comparison with the

experimental data. The strain rate dependence of the tensile behavior of this alloy at 950°C is also demonstrated in Fig. 5. The parameters for this material model are given in Table 1.

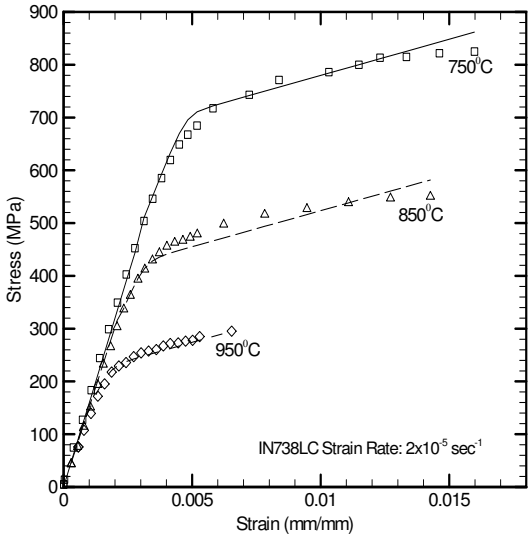

Fig. 4. Stress-strain curves for the IN738LC with the lines as described by Eq. (22).

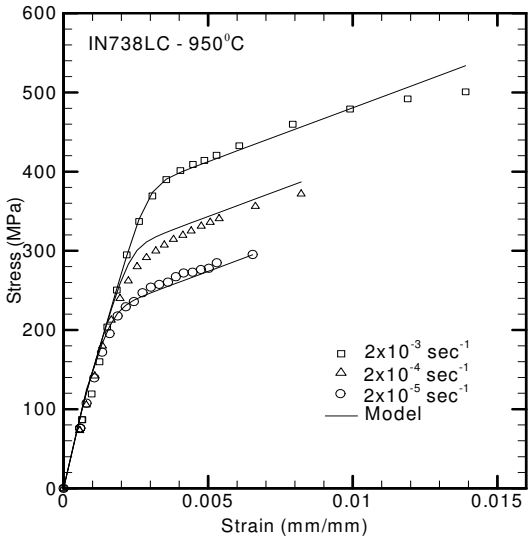

Fig. 5. Stress-strain responses of IN738LC to different loading strain rates at 950 °C.

Temperature (°C)	750	850	950
Initial lattice resistance, σ_0 (MPa)	540	285	110
Work Hardening Coefficient, H (MPa/mm/mm)	15000	13736	12478
Modulus of Elasticity, E (GPa)	175.5	151.4	137.0
Strain-Rate Constant, $A = A_0 \exp[-\Delta G_0^{\neq}/kT]$ (sec^{-1})	3.5×10^{-8}	1.56×10^{-7}	5.5×10^{-7}
Activation Constants			
Activation Volume, V (m^3)	3.977×10^{-22}		
Pre-exponential, A_0 (sec^{-1})	0.7		
Activation Energy, $\Delta G_0^{\neq}$ (J)	2.38×10^{-19}		

Table 1. Constitutive Model Parameters for IN738LC

This constitutive model has 6 parameters: E, H, V, σ_0, A_0 and $\Delta G_0^{\neq}$, which have defined physical meanings. The elastic modulus, E, the work-hardening coefficient, H and the initial activation stress σ_0, are temperature-dependent. The activation parameters, V, A_0 and $\Delta G_0^{\neq}$, are constants corresponding to a "constant microstructure". As far as deformation in a lifing process is concerned, which usually occurs within a small deformation range of ±1%, the description is mostly suffice. The present model, in the context of Eq. (22), also incorporates some microstructural effects via H and σ_0. The significance will be further discussed later when dealing with fatigue life prediction. But before that, let us examine the cyclic deformation process as follows.

Under isothermal fully-reversed loading conditions, first, Eq. (22) describes the monotonic loading up to a specified strain. Upon load reversal at the maximum stress point, the material has $2\sigma_0 + H\varepsilon_p$ as the total stress barrier to yield in the reverse cycle. This process repeats as the cycling proceeds. As an example, the hysteresis loop of IN738LC is shown in Fig. 6. The solid line represents the model prediction with the parameters given in Table 1 (except σ_0 = 40 MPa for this coarser grained material). The model prediction is in very good agreement with the experimental data, except in the transition region from the elastic to the steady-state plastic regimes, which may be attributed to the model being calibrated to a finer-grained material.

As Eq. (22) implies, material deforms purely elastically when the stress is below σ_0, but plasticity starts to accumulate just above that, which may still be well below the engineering yield surface defined at 0.2% offset. This means that the commencing of plastic flow may first occur at the microstructural level, even though the macroscopic behaviour still appears to be in the elastic regime. In this sense, σ_0 may correspond well to the fatigue endurance limit. Therefore, just by analyzing the tensile behaviour with Eq. (22), one may obtain an important parameter for fatigue life prediction.

Tanaka and Mura (Tanaka & Mura, 1981) have given a theoretical treatment for fatigue crack nucleation in terms of dislocation pile-ups. Fig. 7 shows a schematic of crack nucleation by a) vacancy dipole, which leads to intrusion; b) interstitial dipole which leads to extrusion, or c) tripole that corresponds to an intrusion-extrusion pair. They obtained the following crack nucleation formula:

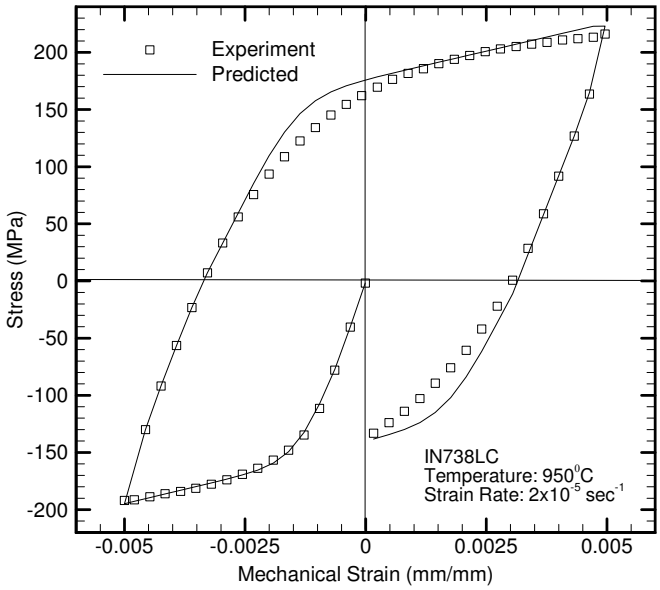

Fig. 6. Hysteresis loop of IN738LC at 950°C.

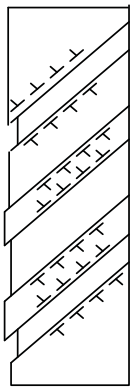

(a) vacancy dipole

(b) interstitial dipole

(c) tripole

Fig. 7. Dislocation pile-ups by (a) vacancy dipoles (intrusion), (b) interstitial dipoles (extrusion) and (c) tripoles (intrusion-extrusion pair).

$$N_c = \frac{4(1-\nu)w_s}{\mu b}\frac{1}{\Delta\gamma^2} \tag{24}$$

where $\Delta\gamma$ is the plastic shear strain range.
Under strain-controlled cycling conditions, $\Delta\varepsilon_p = \Delta\varepsilon - \Delta\sigma/E$, Eq. (24) can also be written in the following form:

$$\frac{1}{N} = C\varepsilon_p^2 = C\left(\Delta\varepsilon - \frac{\Delta\sigma}{E}\right)^2 \tag{25}$$

Fig. 8 shows the prediction of Eq. (25) with C = 0.009 for fully-reversed low cycle fatigue of IN738 at 400°C, in comparison with the experimental data (Fleury & Ha, 2001). The flow stress σ is obtained from Eq. (22). Since the tensile behaviour of IN738 exhibits no significant temperature dependence below 700°C, the material properties at 750°C, as listed in Table 1, are used for the evaluation. Apparently, according to Eq. (25), the material's fatigue life approaches infinity when the total strain $\varepsilon \to \sigma_0/E$. In this case, the predicted endurance limit σ_0/E is approximately 0.4, which agrees well with the experimental observation. As shown in Fig. 8, when the fatigue life is correlated with the plastic strain range, the relationship is represented by a straight line in the log-log scale, as established by Coffin (1954) and Mansion (1954), through numerous experimental observations on metals and alloys. When the fatigue life is correlated with the total strain range, the relationship becomes nonlinear.

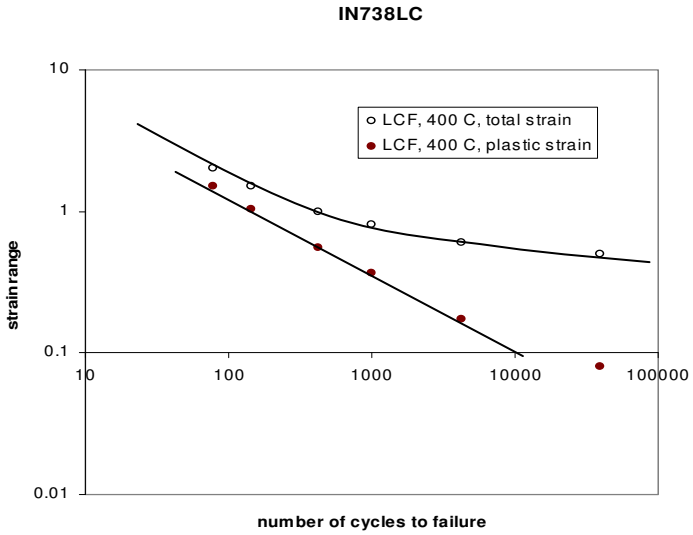

Fig. 8. LCF life of IN738 in terms of plastic and total strain (%).

The nonlinear total-strain-based fatigue life equation is often written as:

$$\Delta\varepsilon_p = \varepsilon'_f N_f^c + \frac{\sigma'_f}{E} N_f^b \tag{26}$$

where c, b, ε'_f and σ'_f are empirical constants.

Eq. (26) has been extensively used by engineers analyzing fatigue data. To establish the relationship, one needs to conduct strain-controlled cyclic tests with appreciable plastic deformation, and also stress controlled cyclic tests when plasticity is not measurable. Arbitrarily, failure cycles less than 10^4 has been termed *low cycle fatigue* (LCF), and above that *high cycle fatigue* (HCF). Laboratory LCF data are usually used to estimate the life of component with stress concentration features such as notches and holes, since it is believed that with the constraint of the surrounding elastic material, the local deformation behaviour is leaning more towards strain-controlled condition; whereas HCF data are usually used to

assess the component life under elastic stresses. For gas turbine engine components, an LCF cycle may represent major loading cycles such as engine start up -shutdown. HCF, on the other hand, occurs under low-amplitude cyclic stresses where deformation is primarily elastic. HCF failures are usually associated with vibration-induced stresses due to mistune or other geometrical damage that change the vibration characteristics of the component. It can become a life-threatening mode of failure especially when it is superimposed on LCF induced cracks. Under these conditions, components vibrate with high frequencies that can reach thousands of cycles per second, and hence exhaust its fatigue life after a short period of time.

Eq. (25) can also be extrapolated to HCF under stress controlled fatigue conditions. When the applied stress is well below the engineering yield point, the logarithm term in Eq. (22) is nearly zero such that the plastic strain can be approximated by

$$\varepsilon_p \approx \frac{\sigma - \sigma_0}{H} \tag{27}$$

and Eq. (25) can be rewritten as

$$\sigma = \sigma_0 + H(BN)^{-1/2} \tag{28}$$

Fig. 9 shows the S-N relationship of Ti-6Al-4V described with Eq. (28). In summary, it has been show that Eq. (25) can be used for both LCF and HCF regimes with the material constitutive law, Eq. (22). It can potentially simplify the fatigue analysis by calibrating with a few cyclic tests in either LCF or HCF regime.

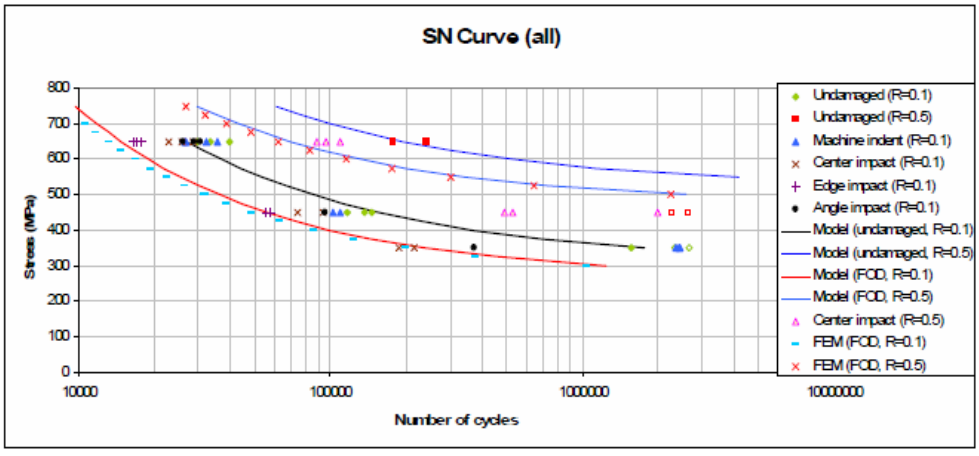

Fig. 9. S-N curves of Ti6Al4V under pristine and foreign object damaged conditions (Wu, 2009a).

3.2 Thermomechanical fatigue

Advanced turbine blades and vanes often employ a sophisticated cooling scheme, in order to survive at high firing temperatures. During engine start up and shutdown, these components experience thermal-mechanical cyclic loads, which can have a severer impact

on the life of the material than isothermal conditions. Thermomechanical fatigue (TMF) refers to the fatigue behaviour of a material under simultaneously thermal and mechanical loads. For laboratory studies, usually simple TMF cycles are employed: i) the in-phase (IP) cycle, which has a 0° phase angle between thermal and mechanical loads; ii) the out-of-phase (OP) cycle, which has a 180° phase angle; and iii) the diamond phase (DP) cycle, which has a phase angle in between; as schematically shown in Fig. 10. The OP and IP cycles represent two extreme conditions, where the maximum stress is reached at the "hot" end of IP and the "cold" end of OP temperature cycle. A more sophisticated engine cycle is shown in Fig. 11, which consists of a half diamond-phase cycle, a thermal excursion from T_{mean} to T_{max}, and a hold period at the maximum load.

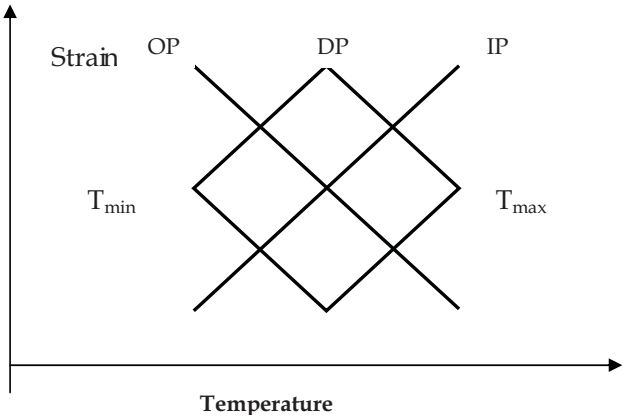

Fig. 10. Temperature-strain cycles for different TMF tests.

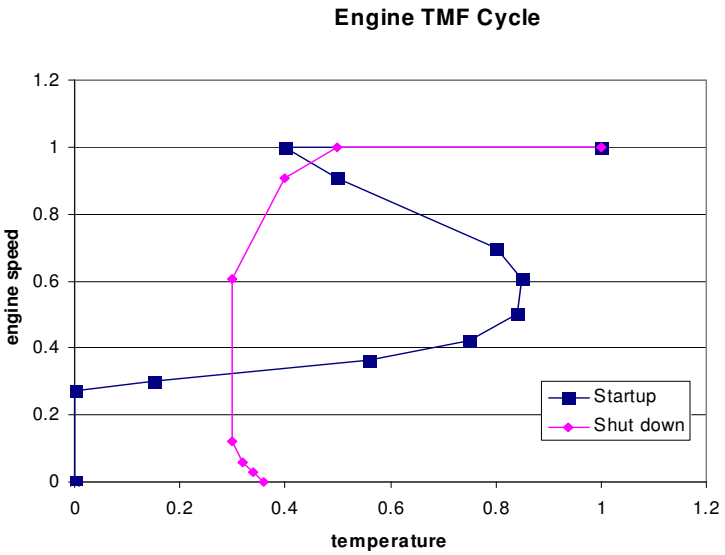

Fig. 11. An engine TMF cycle.

During TMF, the total strain (ε_{tot}) is the sum of thermal and mechanical strain components:

$$\varepsilon_{tot} = \varepsilon_{th} + \varepsilon_{mech} = \alpha(T - T_0) + \varepsilon_{mech} \tag{29}$$

where ε_{th} is the thermal strain, T_0 is the reference temperature, T is the current temperature, and α is the thermal expansion coefficient. The mechanical strain (ε_{mech}) in general can be considered as the sum of the elastic and inelastic strain components.

The damage accumulation and interactions during TMF can be very complex, because it usually involves fatigue, oxidation and creep in some combination. In extreme cases, the combined effects of temperature and stress could just induce one dominant damage mode, for example, it is generally believed that the IP cycle produces predominantly creep damage, while the OP cycle induces oxide-scale cracking (Sehitoglu, 1992). However, under general TMF conditions, the combined damage mechanisms and their interactions can be complicated. Many factors such as the maximum and minimum temperature, thermal and mechanical strain ranges, the phasing between temperature and strain, the strain rate, dwell time, and environment can all influence TMF life. It is almost a formidable task to characterize these effects completely by experimental approaches such as those adopted for LCF and HCF assessments. Therefore, physics based models are needed to describe the complex damage processes under TMF loading. In this section, the cyclic thermomechanical deformation behaviour is described. Interactions with oxidation and creep under general TMF conditions will be discussed later.

For TMF, we assume that the evolution of the energy, Ψ, undergoes a series of infinitesimal isothermal steps, for each i-th step, the energy state evolves from Ψ_{i-1} to Ψ_i over the time interval $\Delta t_i = t_i - t_i\text{-}1$ at a constant temperature T_i. Then, Eq. (18) can be integrated into the form:

$$\ln\left(\frac{e^{-\Psi} - a}{\chi e^{-\Psi} + b}\right)\Bigg|_{\Psi_{i-1}}^{\Psi_i} = -\frac{VE\dot{\varepsilon}\sqrt{1+\chi^2}}{kT_i}\Delta t_i \qquad (i=1,2,\ldots) \tag{30}$$

Summing up all these infinitesimal steps, we have:

$$\sum_{i=1}^{N} \ln\left(\frac{e^{-\Psi} - a}{\chi e^{-\Psi} + b}\right)\Bigg|_{\Psi_{i-1}}^{\Psi_i} = -\sum_{i=1}^{N} \frac{VE\dot{\varepsilon}\sqrt{1+\chi^2}}{kT_i}\Delta t_i \tag{31}$$

Let $N\to\infty$, the left-hand side of Eq. (31) will be equal to the logarithmic difference between the final state and the initial state, and the right-hand side is an integration of the temperature-dependent terms over the loading period. After mathematical rearrangement, we have:

$$\left(\frac{e^{-\Psi} - a}{\chi e^{-\Psi} + b}\right) = \left(\frac{1-a}{\chi + b}\right)\exp\left\{-\int_{t_0}^{t} \frac{V\mu\dot{\gamma}\sqrt{1+\chi^2}}{kT}dt\right\} \tag{32}$$

where t_0 is the time to reach the elastic limit, or in other words, for plastic flow to commence, as defined by Eq. (21).

Let

$$\omega(t) = \left(\frac{1-a}{\chi+b}\right)\exp\left\{-\int_{t_0}^{t}\frac{VE\dot{\varepsilon}\sqrt{1+\chi^2}}{kT}dt\right\} \tag{33}$$

and assume that within the temperature range of TMF, the variation of E is moderate such that it can be represented by its average E_m, and $\sqrt{1+\chi^2} \approx 1$ since χ is usually small, the ω function can be evaluated as,

$$\omega = \left(\frac{1-a}{\chi+b}\right)\exp\left\{\mp\frac{VE_m\Delta\varepsilon\sqrt{1+\chi^2}}{k\Delta T}\ln\frac{T}{T_0}\right\} \tag{34}$$

where $\Delta T = T_{max} - T_{min}$ is the temperature range, $\Delta\varepsilon$ is the total strain range, the -/+ sign is used for the temperature rising or declining halves of the cycle, respectively, and T_0 denotes the temperature point at which the stress reaches the elastic limit, which can be determined based on the thermomechanical cycle profile, i.e., the T - ε relationship.
Then, Eq. (32) can be rewritten into the stress vs. strain function, similar to Eq. (22), as

$$\sigma - H\varepsilon_p - \sigma_0 = -\frac{kT}{V}\ln\left(\frac{a+\omega b}{1-\omega\chi}\right) \tag{35}$$

The stress-strain response of the coarse-grained IN738LC under an out-of-phase thermomechanical fatigue condition is predicted using Eq. (35), as shown in Figure 2.10, with the parameter values given in Table 2.1 but with a reduced σ_0 =40MPa for the coarse-grained (d~5mm) material. The predicted hysteresis loop is in good agreement with the experimentally measured response.

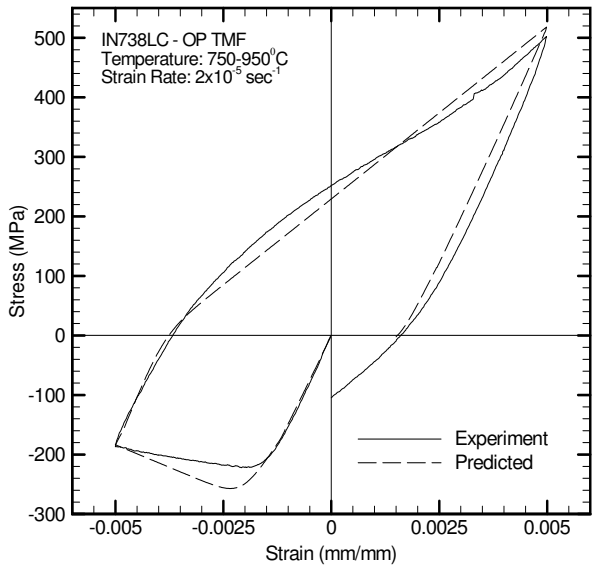

Fig. 12. Stress-strain response of IN738LC (coarse-grain) during an OP-TMF cycle.

3.3 Creep

Creep is a mode of inelastic material deformation occurring under sustained loading at high temperatures, usually above 0.3 T_m (T_m is the material's melting point). Creep can be one of the critical factors determining the integrity of components at elevated temperatures. In gas turbine engines, especially in hot sections, components such as turbine blades are subjected to sustained loads (centrifugal force and pressure) at high temperatures during the operation. Creep of a turbine blade can also cause dimensional changes that either reduce its aerodynamic efficiency or lead to elongation that rubs the engine casing, which may induce additional vibration and noise. Furthermore, creep damage may interact with fatigue that leads to significant reduction in the service life of the component.

Creep mechanisms have been extensively reviewed (Frost & Ashby, 1982; Ashby & Dyson, 1985; Wu & Koul, 1996). It is generally understood that the creep rate has different stress dependence by different mechanisms. Nevertheless, the steady-state creep rate (or the minimum creep rate) is often expressed in a Norton-Bailey form, as

$$\dot{\varepsilon} = A_0 \exp\left(\frac{Q}{RT}\right)\sigma^n \tag{36}$$

where Q is the activation energy, T is the absolute temperature, R is the universal gas constant, and A_0 and n are empirical constants.

Traditionally, creep damage assessment has been mainly based on the minimum creep rate and the Larson-Miller plot, taking into consideration the temperature compensated rate property as exhibited in Eq. (36). Fig. 13 shows the Larson-Miller plot for Astroloy. In general, the stress vs. Larson-Miller parameter relationship is nonlinear due to the multiple creep mechanisms involved, and therefore, it is merely an experimental correlation rather than a physics-based model. Extrapolation to predict the long term creep life using Larson-Miller parameter has to be based on extensive testing. For component life prediction, it needs a constitutive law of creep to describe the stress relaxation and redistribution with time as creep deformation proceeds.

It has been known that creep deformation is a continuous physical process, where a decreasing creep rate regime (transient creep: primary plus secondary) is followed by an accelerating creep rate regime (tertiary creep) beyond a minimum creep rate. Wu & Koul (1996) have proposed a creep-curve model, based on the decomposition of the total inelastic strain into grain boundary sliding and intragranular deformation, as expressed in Eq. (1), and concluded that grain boundary sliding is primarily responsible for the transient creep behaviour, while the tertiary creep evolves mostly intragranular deformation with dislocation multiplication.

Under uniaxial loading condition, the solution of Eq. (8)-(14) has the form (Wu & Koul, 1995)

$$\varepsilon_{gbs} = \varepsilon_0 + \phi\dot{\varepsilon}_{ss}t + \frac{\sigma}{\beta^2 H_{gbs}}\left[1 - \exp\left(-\frac{\beta^2\phi H_{gbs}\dot{\varepsilon}_{ss}t}{\sigma(\beta - 1)}\right)\right] \tag{37}$$

where β is a microstructure parameter, and

$$\dot{\varepsilon}_{ss} = \varphi(1-\beta^{-1})\frac{D\mu b}{kT}\left(\frac{b}{d}\right)^q\left(\frac{l+r}{b}\right)^{q-1}\frac{\sigma(\sigma-\sigma_{ic})}{\mu^2} \tag{38}$$

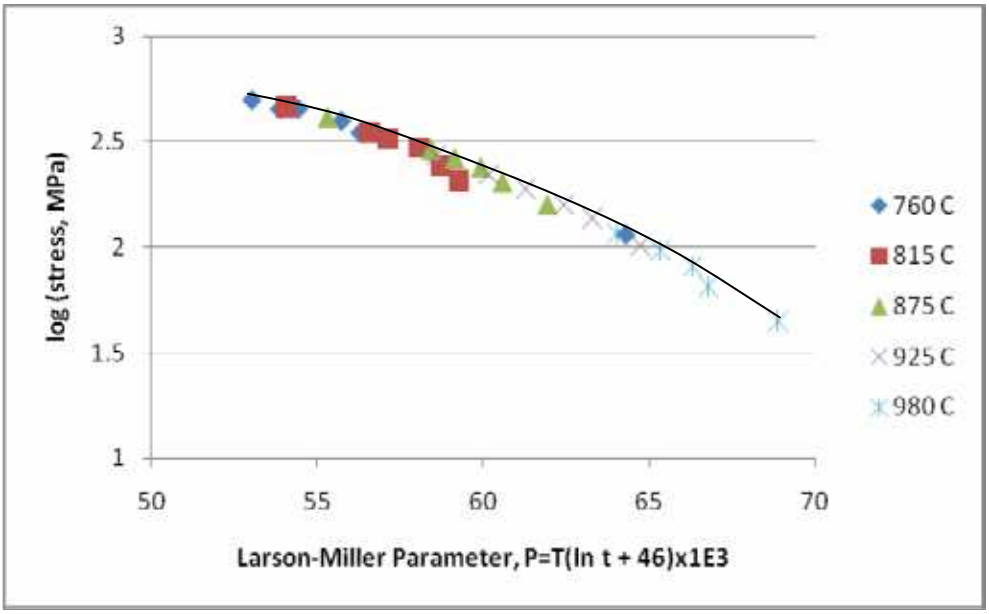

Fig. 13. The Larson –Miller plot for Astroloy.

Equation (37-38) is derived from the grain boundary dislocation glide plus climb mechanism. It states that the transient creep is a grain boundary sliding phenomenon that consists of a primary stage and a steady-state stage. It is influenced mostly by grain boundary microstructure and morphology, thus emphasizing the importance of grain boundary engineering in alloy design. According to Eq. (37), the true steady-state creep occurs at a rate as described by Eq. (38) only after an infinitely long time. Practically, a quasi-steady-state may be observed relatively soon after creep deformation starts, since the primary strain is reached as an exponential function of time. However, how long the quasi-steady-state will last depends on the time to the onset of tertiary creep, which is controlled by damage accumulation in both grain interior and along grain boundaries, such as dislocation multiplication, precipitate coarsening and cavity nucleation and growth. These processes may eventually take over and lead to an acceleration in the creep rate. Tertiary creep phenomena will be discussed later. Presently, we will discuss the important characteristics of transient creep before the commencing of tertiary creep.
First of all, the present model predicts a primary strain, as defined by

$$\varepsilon_{tr}^{p} = \frac{\sigma}{\beta^2 H_{gbs}} \tag{39}$$

It states that the primary strain is proportional to the applied stress σ divided by the work hardening coefficient H_{gbs}. This relationship may provide guidance for grain boundary engineering to lower the primary strain in alloy applications. Practically, the primary strain can be attained ~99 percent when the exponential term reaches 4.6, which defines the primary time as follows.